Proceedings of the 2015 European School of High-Energy Physics, Bansko, Bulgaria, 2 – 15 September 2015, edited by M. Mulders and G. Zanderighi, CERN Yellow Reports: School Proceedings, Vol. 4/2017, CERN-2017-008-SP (CERN, Geneva, 2017)

A very brief Introduction to Heavy Ion Physics

S. Floerchinger[*]
Institut für Theoretische Physik, Universität Heidelberg, Heidelberg, Germany

Abstract
Relativistic heavy ion collisions provide a possibility to investigate a fundamental quantum field theory (QCD) in a regime away from the conventional vacuum, namely at non-zero temperature and density. I will discuss why this is important, give a brief overview over what is known already and also mention currently still open questions.

Keywords
Lectures; ESHEP; Heavy ion collisions; Quark-gluon plasma.

1 Motivation and introduction

Why should one be interested in heavy ion collisions? There are several reasons. An experimentalist may argue: Heavy ion collisions at high energy provide a possibility to experimentally address questions like: What happens with Quantum Chromodynamics (QCD) at large density or temperature? Is there, for example, a phase transition at the Hagedorn temperature?

From a more theoretical point of view one may say: Quantum field theory is so important for the description of the phenomena in our world that it should be studied and understood not only in the regime of a few particles or excitations around the conventional vacuum but also at non-vanishing temperature and density. This is also important for many questions in cosmology and in condensed matter theory. Heavy ion collisions allow to study one of the fundamental building blocks of the standard model (namely QCD) at non-zero temperature and density. This is particularly interesting due to the asymptotic freedom property of QCD. For very large momenta or at very small distances, the theory is theoretically very well understood. Once the Lagrangian of QCD is fixed in terms of the fundamental parameters (the strong coupling constant α_s and the quark masses) everything else is in principle determined, as well, including the thermal equilibrium properties and even the non-equilibrium dynamics. It is a formidable challenge to understand this in detail and to solve the corresponding equations in practice.

From a cosmologists perspective one may argue that the quark gluon plasma is interesting because it has filled the universe from about 10^{-12} to 10^{-6} seconds after the big bang. Heavy ion collisions allow to learn something about this state of matter from laboratory experiments.

Finally, heavy ion physics is a very active field of research. A large experimental program is ongoing at the Large Hadron Collider (LHC) at CERN, Geneva, Switzerland, with experimental research being performed by the collaborations ALICE, ATLAS, CMS and LHCb. Another large program is ongoing at the Relativistic Heavy Ion Collider (RHIC) at Brookhaven National Laboratory (BNL) in Brookhaven, USA, with experimental collaborations Phenix and STAR. Future experiments are planned at the Facility for Antiproton and Ion Research (FAIR) in Darmstadt, Germany, and at the Nuclotron-based Ion Collider Facility (NICA) at JINR, Dubna, Russia.

We end this introductory section with a brief overview on the different regimes following a heavy ion collision event. The initial state directly after the collision is determined in principle by the wave function of the colliding nuclei. However, the latter is unfortunately not understood from first principles yet. (The problem is of considerable complexity already for protons.) Directly after the collision there must be a regime of strong dynamics driving an approximate thermalization (or at least

[*]Previous affiliation: CERN, Geneva, Switzerland

https://doi.org/10.23730/CYRSP-2017-004.141

pre-thermalization sometimes also called "hydrodynamization" such that the energy-momentum tensor approaches the form of relativistic fluid dynamics). The concrete dynamics is not yet known in all details but it is very plausible that strong color fields play an important role as well as possibly different plasma instabilities.

Afterwards there is a phase with (approximate) local thermal and chemical equilibrium that can be described by relativistic fluid dynamics. The strong microscopic dynamics that leads to short equilibration times is now responsible for rather small dissipative transport coefficients (such as shear viscosity and corresponding relaxation times, see discussions below). The main characteristic of the fluid dynamic phase is a rapid expansion both in longitudinal and transverse direction and an associated dilution and cool down of the fluid.

Together with the dilution comes a change in the relevant microscopic degrees of freedom. While these are gluons and quarks at high temperatures, mesons and baryons dominate the low temperature and density phase. As long as the densities are still rather large, there are many inelastic (and elastic) collisions such that chemical and kinetic equilibrium are maintained. When the density drops, the rate of inelastic collisions decreases and at some point becomes too small to maintain chemical equilibrium. This process is called chemical freeze-out. After this point the total particle yields do not change substantially any more (except by some resonance decays that are ongoing). One can still use an (approximate) fluid dynamic description in the phase that follows, but now with a chemical potential for each (separately) conserved particle number.

Finally, when the densities drop even further, also elastic collisions become more and more rare such that also kinetic equilibrium is no longer maintained. After this point also the momenta of particles do not change substantially any more (again with the exception of resonance decays) and they are "free streaming" towards the detector. This process is described as kinetic freeze-out. More details about both chemical and kinetic freeze-out will be discussed below.

There are some very good reviews and monographs on heavy ion physics which are much more detailed than I can possibly be in these introductory lectures, for example refs. [1–6]. A very helpful source of information are also the collected proceedings of the "Quark Matter" conferences.

For these lecture notes I will mainly employ relativistic natural units with $c = \hbar = k_B = 1$.

2 Basic quantum chromodynamics

We now continue with a very basic reminder about the microscopic properties of QCD as a quantum field theory. The Lagrangian is

$$\mathscr{L} = -\frac{1}{2}\text{tr}\ \mathbf{F}_{\mu\nu}\mathbf{F}^{\mu\nu} - \sum_f \bar{\psi}_f \left(i\gamma^\mu \mathbf{D}_\mu - m_f\right)\psi_f \tag{1}$$

with matrix valued field strength tensor $\mathbf{F}_{\mu\nu} = \partial_\mu \mathbf{A}_\nu - \partial_\nu \mathbf{A}_\mu - ig[\mathbf{A}_\mu, \mathbf{A}_\nu]$ and covariant derivative $\mathbf{D}_\mu = \partial_\mu - ig\mathbf{A}_\mu$. In the high energy regime, where perturbation theory is valid, the particle content of the theory are $N_c^2 - 1 = 8$ real massless vector bosons, the gluons, and $N_c \times N_f$ massive Dirac fermions, the quarks. From the quark masses (Up 2.3 MeV, Down 4.8 MeV, Strange 95 MeV, Charm 1275 MeV, Bottom 4180 MeV and Top 173 GeV) one can see that for typical temperatures in the regime of a few 100 MeV mainly the Up, Down and Strange quarks play a role as thermalized particles while Charm and Bottom can be considered as heavy. Top quarks can be counted as very heavy.

An important feature of QCD is asymptotic freedom. The coupling constant $\alpha_s = g^2/(4\pi)$ has a renormalization group running such that the effective interaction strength is small for processes with large momentum transfer or at high energy scales. On the other side, the effective interaction strength becomes large for soft processes or at small energy scales. An illustration of this is given by Fig. 1.

From this one concludes generically that at high-temperatures QCD should have the properties of a weakly coupled field theory while it becomes effectively strongly coupled at small temperatures. This

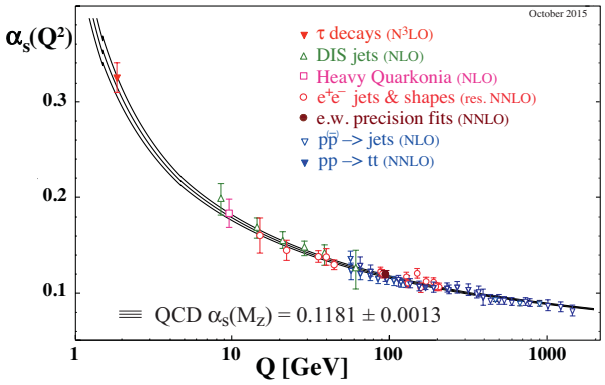

Fig. 1: Summary of measurements of α_s as a function of the energy scale Q as compiled by the Particle Data Group in 2015. Figure taken from ref. [7].

is so for a description in terms of the elementary degrees of freedom (quarks and gluons). In terms of the composite degrees of freedom that dominate at low temperatures (mesons and baryons) the situation is different and in particular the low temperature regime permits a description which resembles in many aspects a weakly coupled theory.

This brings us to the next important property of QCD: confinement. For low temperatures, quarks and gluons are confined to hadrons. In contrast, the large temperature behavior is dominated by deconfined quarks and gluons. Lattice QCD calculations have shown that the intermediate regime does not show a sharp (first or second order) phase transition but rather a continuous crossover.

3 Particle production in heavy ion collisions

When heavy ions are colliding at large center of mass energy, many particles are being produced. Consider for example the first heavy ion run at the LHC. The total collision energy for the Pb-Pb system is $\sqrt{s} = 2 \times 574$ TeV. The fully ionized nuclei ^{208}Pb consist of 82+126=208 nucleons. This implies a collision energy per nucleon of $\sqrt{s}_{\rm NN} = \frac{574}{208}$ TeV = 2.76 TeV.

Lower energy experiments performed at the Alternating Gradient Synchrotron (AGS) operating at BNL since the mid 1980's reached typical values $\sqrt{s}_{\rm NN} \approx 2-5$ GeV. For the fixed target experiments at the Super Proton Synchrotron (SPS) at CERN since 1994 the energies are in the range $\sqrt{s}_{\rm NN} < 17$ GeV. Finally the Relativistic Heavy Ion Collider (RHIC) in operation at BNL since 2000 reaches energies $\sqrt{s}_{\rm NN} \leq 200$ GeV.

The number of charged particles found in the detector varies with the longitudinal angle with respect to the beam axis. Usually this angle is parametrized by the pseudo-rapidity $\eta = -\ln(\tan(\theta/2))$. Depending on the coverage of the detector one can access $dN_{\rm ch}/d\eta$ in the range of a few units around mid-rapidity $\eta = 0$. Integration of this function (or an interpolation thereof) gives total number of charged particles $N_{\rm ch}$. A typical number is $N_{\rm ch} = 5060 \pm 250$ at upper RHIC energies. One should keep in mind that not all particles are charged and one can estimate the total number of hadrons as $1.6 \times 5060 \approx 8000$ hadrons in total. The number of produced particles grows with the collision energy and at the LHC one can estimate $N_{\rm ch} = 25000$ corresponding to about 40000 hadrons in total.

Using modern detector technology one can also identify the produced particles and determine the yields or multiplicities for each species separately. Some results are shown in Fig. 2 together with fits based on the so-called statistical or thermal model. The thermal model describes the particle yields in terms of a non-interacting hadron resonance gas in thermal and chemical equilibrium. Essentially all hadrons and resonances listed by the particle data group are included. Fit parameters are the temperature T, volume V and chemical potentials for the conserved baryon number μ_b and similar for isospin,

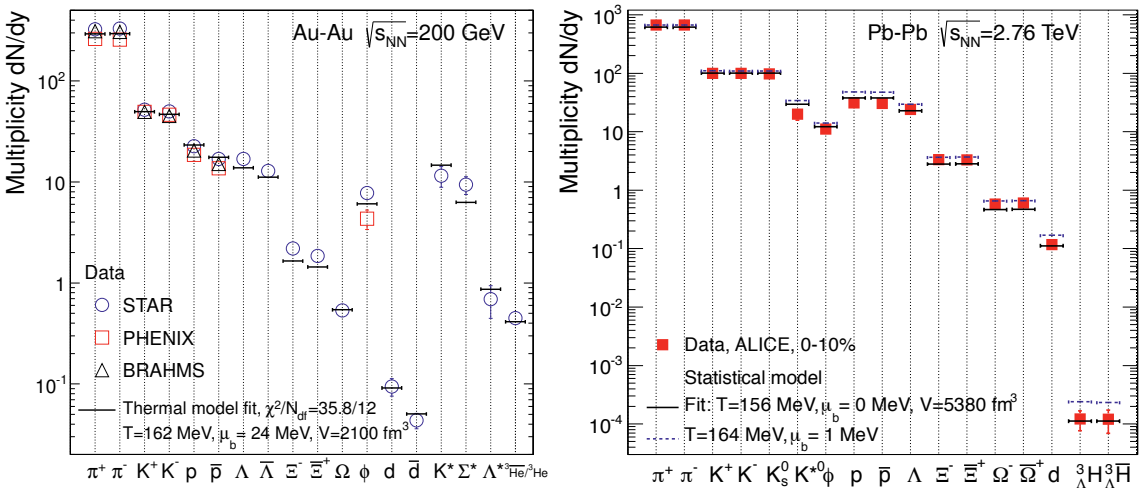

Fig. 2: Comparison of hadron yields as measured at RHIC (left panel) and by ALICE at the LHC (right panel) and fits using the thermal hadronization model. The first figure is taken from ref. [8], the second from ref. [9].

strangeness and charm.

The thermal model works so surprisingly well that a number of questions arise. First of all, why does it actually work so well? Why should all the particle yields be determined by one and the same temperature? One should keep in mind that hadronization is governed by non-perturbative QCD processes that are not completely understood yet. One interpretation is in terms of a sudden chemical freeze-out. The picture is based on a close-to-equilibrium expansion and cool-down of the fluid. Number changing processes are fast when the densities are high and keep up the chemical equilibrium. At lower temperatures these processes become too slow to keep up with the expansion and particle numbers get frozen in. The freeze-out process itself is not describable in a close-to-equilibrium picture but if it happens quickly enough, it is nevertheless possible that the particle yields are frozen in to their thermal values on the "surface of last inelastic scattering". In order to explain the fact that a single temperature accounts for all particle yields, rates of inelastic collisions have to drop rather quickly. It has been argued that this is the case very close to the chiral crossover [10] and indeed, the chemical freeze-out temperatures as determined from the thermal model fits and the crossover temperatures as calculated by lattice QCD seem to be in reasonable agreement for the high energy experiments where the net baryon chemical potential is small. On the other side, this picture seems to be too simple for the experiments at lower energies corresponding to higher baryon number chemical potentials at freeze-out [11]. In Fig. 3 an overview over the chemical freeze-out points in the plane of temperature and baryon chemical potential is given for experiments at various energies together with lattice QCD results about the chiral crossover line.

4 Thermodynamics and fluid dynamics

We now turn to the thermodynamic and fluid dynamic description of the QCD matter that is produced by relativistic heavy ion collisions. As a warm-up let us recapitulate the Stefan-Boltzmann law for the pressure of a gas of N_B species of real, massless bosonic degrees of freedom and N_F real, massless fermionic degrees of freedom

$$p(T) = \frac{\pi^2}{90}\left(N_B + \frac{7}{8}N_F\right)T^4. \tag{2}$$

For QCD at high temperatures one has N_c^2-1 gluons in two helicity states where $N_c = 3$ is the number of colors, i. e. $N_B = 2\times(N_c^2-1) = 16$. In addition, in the temperature regime of relevance, there are $N_f =$

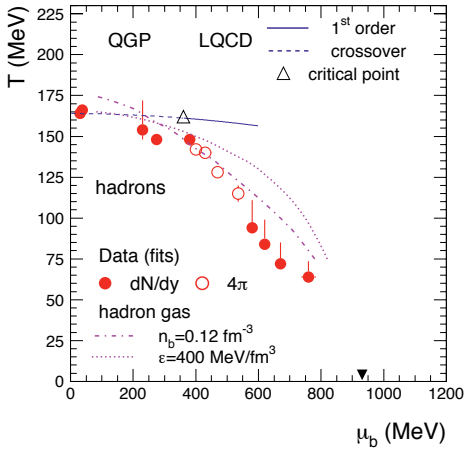

Fig. 3: Values for temperature T and baryon chemical potential μ_b as obtained from thermal fits. The Lattice QCD results are from ref. [12]. The full triangle indicates the location of first order phase transition of normal nuclear matter. The figure is taken from ref. [13].

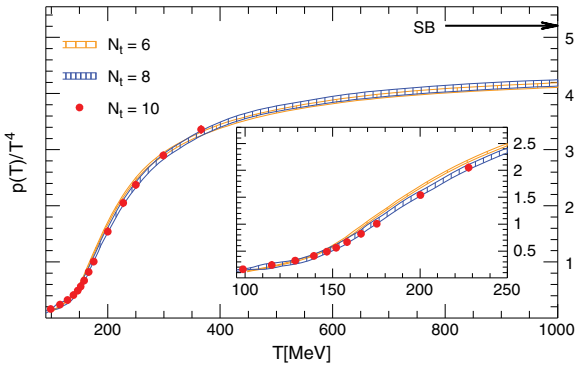

Fig. 4: The "thermodynamic equation of state" or pressure $p(T)$ (divided by T^4) as a function of temperature T as calculated from Lattice QCD. Figure taken from ref. [14].

3 quark flavors that are effectively massless with $N_c = 3$ colors and 2 helicity states. Moreover, quarks are complex fermions corresponding to 2 real degrees of freedom. That gives $N_F = 4 \times N_c \times N_f = 30$.

Corrections to the pressure in eq. (2) arise from the non-vanishing quark masses as well as from interactions. For small temperatures there are fewer effective degrees of freedom. For example, for $M_\pi < T < M_\rho$ one has approximately $N_B = 3$ massless pions and no massless fermions, $N_F = 0$. More general, at low temperature, $p(T)$ can be calculated approximately from a hadron resonance gas. For the transition region between large and small temperatures one needs a non-perturbative calculation of $p(T)$ as it is given by lattice QCD. Fig. 4 shows the result of a lattice QCD simulation at vanishing chemical potentials, which is the regime most relevant for heavy ion collisions at high energies. By the formula of thermodynamics, other quantities such as energy density $\epsilon(T)$, entropy density $s(T)$ and so on can be calculated from the pressure $p(T)$ in terms of the appropriate derivatives and Legendre transforms.

Let us now come to fluid dynamics. Quite generally, if one considers large enough time and length scales and if the interaction effects that drive local thermalization are strong enough, quantum fields form a fluid. A fluid dynamic description is always an approximation which does not describe all particles or degrees of freedom individually, but it is an approximate description that works rather well for many

aspects of heavy ion physics. Fluid dynamics is a rather general framework that allows to describe many different physical phenomena within a common setup and with similar equations. This ranges from conventional liquids such as water to superfluid helium, strongly interacting cold atomic gases, the quark gluon plasma or the cosmological fluid.

However, fluid dynamics it is not a closed theory. It needs input from calculations at a more microscopic level (or corresponding measurements) in terms of some macroscopic material properties. These are first of all the thermodynamic equation of state, i. e. information such as the function $p(T)$ from which one can derive also other thermodynamic quantities. In addition one needs information about transport properties such as the shear viscosity $\eta(T)$, the bulk viscosity $\zeta(T)$, heat conductivity $\kappa(T)$ and at least if one is interested in finer details, one also needs corresponding relaxation times $\tau_{\text{shear}}(T)$, $\tau_{\text{bulk}}(T)$ and other related quantities.

As a theoretical framework, fluid dynamics is organized as an expansion in derivatives. The lowest order is ideal fluid dynamics which we discuss first. The starting point is the energy-momentum tensor of a fluid in *global* thermal equilibrium,

$$T^{\mu\nu} = \epsilon u^\mu u^\nu + p\,(g^{\mu\nu} + u^\mu u^\nu) \tag{3}$$

with (inverse) metric $g^{\mu\nu}$ and fluid velocity u^μ. In Minkowski space and in cartesian coordinates, the metric is a diagonal matrix with entries -1,+1,+1,+1 in our conventions. The fluid velocity is $u^\mu = (1,0,0,0)$ in the reference frame where the fluid is at rest but deviates from this in other frames. It is normalized by $g_{\mu\nu}u^\mu u^\nu = -1$. The pressure p is related to the energy density ϵ by a thermodynamic equation of state, $p = p(\epsilon)$.

Now let us go from *global* thermal equilibrium to *local* equilibrium. The ideal fluid approximation assumes that $T^{\mu\nu}$ is of the form in (3) but now with space and time dependent energy density $\epsilon = \epsilon(x)$ and fluid velocity $u^\mu = u^\mu(x)$. From the conservation law $\nabla_\mu T^{\mu\nu} = 0$ one can obtain evolution equations for $\epsilon(x)$ and $u^\mu(x)$ in ideal fluid dynamics,

$$\begin{aligned} u^\mu \partial_\mu \epsilon + (\epsilon + p)\nabla_\mu u^\mu &= 0, \\ (\epsilon + p) u^\mu \nabla_\mu u^\nu + (g^{\nu\mu} + u^\nu u^\mu)\,\partial_\mu p &= 0. \end{aligned} \tag{4}$$

In these equations, no dissipative effects and in particular no viscosities have been taken into account. This is remedied at the next level of the derivative expansion.

One can decompose a general symmetric energy-momentum tensor as

$$T^{\mu\nu} = \epsilon u^\mu u^\nu + (p + \pi_{\text{bulk}})\Delta^{\mu\nu} + \pi^{\mu\nu} \tag{5}$$

where the shear stress $\pi^{\mu\nu}$ is symmetric, transverse to the fluid velocity, $u_\mu \pi^{\mu\nu} = 0$, and traceless, $\pi^\mu{}_\mu = 0$. The bulk viscous pressure π_{bulk} and shear stress $\pi^{\mu\nu}$ parametrize deviations from ideal fluid dynamics. To first order in derivatives of the fluid velocity one has

$$\begin{aligned} \pi_{\text{bulk}} &= -\,\zeta \nabla_\mu u^\mu + \ldots, \\ \pi^{\mu\nu} &= -\,2\eta \left(\tfrac{1}{2}\Delta^{\mu\alpha}\Delta^{\nu\beta} + \tfrac{1}{2}\Delta^{\mu\beta}\Delta^{\nu\alpha} - \tfrac{1}{3}\Delta^{\mu\nu}\Delta^{\alpha\beta} \right) \nabla_\alpha u_\beta + \ldots, \end{aligned} \tag{6}$$

with bulk viscosity $\zeta = \zeta(\epsilon)$ and shear viscosity $\eta = \eta(\epsilon)$. At second order also the relaxation times $\tau_{\text{shear}}(\epsilon)$ and $\tau_{\text{bulk}}(\epsilon)$ enter, as well as other terms.

Let us now discuss in a little more detail the equations of relativistic viscous fluid dynamics. The evolution equation for energy density becomes for the viscous theory

$$u^\mu \partial_\mu \epsilon + (\epsilon + p + \pi_{\text{bulk}})\nabla_\mu u^\mu + \pi^{\mu\nu}\nabla_\mu u_\nu = 0. \tag{7}$$

The non-relativistic limit $\vec{v}^2 \ll c^2$ gives for the first order approximation

$$\partial_t \epsilon + \vec{v}\cdot\vec{\nabla}\epsilon + (\epsilon + p)\vec{\nabla}\cdot\vec{v} = \zeta \left(\vec{\nabla}\cdot\vec{v}\right)^2 + 2\,\eta\,\sigma_{ij}\sigma_{ij}, \tag{8}$$

with $\sigma_{ij} = \frac{1}{2}\partial_i v_j + \frac{1}{2}\partial_j v_i - \frac{1}{3}\delta_{ij}(\vec{\nabla}\cdot\vec{v})$. The left hand side of this equation describes the change in the fluid's internal energy ϵ by thermodynamic work due to expansion or contraction of the fluid. The right hand side describes the dissipation of the fluid's macroscopic kinetic energy to thermal energy. Using the thermodynamic relations $\epsilon + p = sT$ and $d\epsilon = Tds$ where s is the entropy density, leads to an equation for entropy production

$$\partial_t s + \vec{\nabla}\cdot(s\vec{v}) = \frac{\zeta}{T}\left(\vec{\nabla}\cdot\vec{v}\right)^2 + \frac{2\eta}{T}\,\sigma_{ij}\sigma_{ij}. \tag{9}$$

A local form of the second law of thermodynamics says that the entropy can never decrease. Accordingly, the right hand side of eq. (9) must be positive semi-definite. This implies in particular $\zeta \geq 0$ and $\eta \geq 0$.

The evolution equation for the fluid velocity becomes for the viscous theory

$$(\epsilon + p + \pi_{\text{bulk}})\,u^\mu \nabla_\mu u^\nu + \Delta^{\nu\mu}\,\partial_\mu(p + \pi_{\text{bulk}}) + \Delta^\nu{}_\alpha \nabla_\mu \pi^{\mu\alpha} = 0. \tag{10}$$

The non-relativistic limit of this equation gives for the first order approximation the non-relativistic Navier-Stokes equation (ρ is the mass density which is well defined for a non-relativistic fluid)

$$\rho\left[\partial_t v_j + \vec{v}\cdot\vec{\nabla}v_j\right] + \partial_j p = \partial_j\big(\zeta\vec{\nabla}\cdot\vec{v}\big) + \partial_m\big(2\,\eta\,\sigma_{jm}\big). \tag{11}$$

In this equation, the second term on the left hand side describes acceleration by pressure gradients. The terms on right hand side describe damping by viscosity. More general than the first order approximation, the equations for ϵ and u^μ which follow from the conservation law $\nabla_\mu T^{\mu\nu} = 0$, get closed by relations for π_{bulk} and $\pi^{\mu\nu}$, the so called constitutive relations.

Let us now discuss the transport properties that enter fluid dynamics. For a fluid without any conserved charges besides energy and momentum, such as the quark gluon plasma at negligible net baryon number density, the most relevant transport properties are shear and bulk viscosity. The physical mechanism underlying viscosity is the microscopic transport of momentum. Typically, the momentum is transported out of a local fluid cell by diffusive processes which involve particles, radiation or more general quasi-particles. The strength of shear viscosity can be quantified in terms of the ratio η/s. In order for this ration to become large, momentum must be transported efficiently over distances $s^{-1/3}$ by well defined quasiparticles. On the other side, theories with small η/s have no well defined quasiparticles.

In general, transport properties like shear viscosity, bulk viscosity, heat conductivity, relaxation times, etc. are difficult to determine from quantum field theory. Lattice QCD calculations in Euclidean space cannot determine them directly and the analytic continuation from Euclidean to Minkowski space is numerically very difficult. Concrete expressions can be obtained for very weakly interacting theories from perturbation theory (or from a mapping to kinetic theory) or for strongly interacting theories with gravity dual via the AdS/CFT correspondence. For theories that are neither very weakly nor very strongly interacting, the determination of transport properties is essentially an open problem.

An example, where the viscosities are known, is a dilute simple non-relativistic gas with elastic two-to-two collisions. Here one can obtain from kinetic theory

$$\eta = \tau_{\text{f}}\, n\, T, \tag{12}$$

with particle density n, temperature T, and mean free time

$$\tau_{\text{f}} = \frac{1}{\sigma_{\text{tot}}\,\bar{v}\,n}. \tag{13}$$

In the last equation, σ_{tot} is the total elastic cross section and $\bar{v}$ the mean square velocity of the particles with respect to the fluid velocity. Using $T = \frac{1}{3}m\bar{v}^2$ gives

$$\eta = \frac{m\,\bar{v}}{3\,\sigma_{\text{tot}}}. \tag{14}$$

Interestingly, the shear viscosity becomes large for small cross-section! The bulk viscosity vanishes for the simple non-relativistic gas, $\zeta = 0$.

For QCD, the transport properties can be determined at very high temperature where QCD becomes weakly coupled, $g \ll 1$. The shear viscosity at leading logarithmic accuracy is [15]

$$\eta(T) = k(N_f) \frac{T^3}{g^4 \ln(1/g)}. \tag{15}$$

The bulk viscosity is related to this via the velocity of sound c_s [16]

$$\zeta(T) \approx 15\eta(T) \left(\tfrac{1}{3} - c_s^2(T)\right)^2. \tag{16}$$

For very high temperature $c_s^2 \to 1/3$ and $\zeta \to 0$.

One can also determine the transport properties for a class of strongly interacting field theories which have a gravitational dual in the sense of the AdS/CFT correspondence. It was found that for conformal theories with gravitational dual one has $\eta(T) = s(T)/(4\pi)$ [17]. This was later conjectured to be a universal lower bound for any fluid [18],

$$\frac{\eta}{s} \geq \frac{\hbar}{4\pi k_B}. \tag{17}$$

(We have restored units $\hbar$ and k_B to make the quantum nature of this conjectured bound apparent.) Meanwhile, theoretical counterexamples have been found but experimentally, no system seems to violate the bound so far.

For some theories with deviations from conformal symmetry it was found that the bulk viscosity is related to the shear viscosity by $\zeta(T) = 2\eta(T) \left(\frac{1}{3} - c_s^2(T)\right)$ [19] but this does not seem to be a universal relation.

Ultimately, one would like to gain a theoretical understanding of the shear and bulk viscosity (and related relaxation times) of QCD for the whole range of temperatures. It is possible to write down formal expressions (so called Kubo relations) which express the transport coefficients in terms of correlation functions that can in principle be determined in terms of functional integral expressions. However, it is in practice rather difficult to solve the corresponding equations. Nevertheless, some theoretical attempts in this direction are currently ongoing, using for example the analytic continuation of lattice QCD results [20, 21] or functional renormalization group calculations [22, 23].

5 Fluid dynamics of the fireball for more and more realistic initial conditions

In this section we will discuss the actual solution of relativistic viscous fluid dynamics for the fireball created by two colliding heavy ions. It is obvious that these solutions depend on the initial conditions as they are specified at some early time where the fluid dynamic description is initialized. It would be great to know these initial conditions in detail, for example from first principle calculations in QCD. This is however a very difficult problem by itself. So for the time being, the detailed initial conditions are not known but some of their properties are.

Generically, solutions of partial differential equations as the ones of fluid dynamics are easier to find when the initial conditions are more symmetric. We will therefore start our discussion with particularly symmetric and therefore simple situations although they are not fully realistic. We will then increase the complexity step by step and thereby become more and more realistic.

We start by considering the fluid velocity in the longitudinal direction z, i. e. in the direction parallel to the beam axis. What should be the fluid velocity in that direction as a function of time and space coordinates? It was first argued by Bjorken that a good guess should be $v_z = z/t$ where

the longitudinal position z and the time t are defined such that the actual collision took place at the coordinate origin, i. e. at $z = t = 0$. Note that due to the high energy, the ions are strongly Lorentz contracted in the longitudinal direction such that to good approximation one can speak of a collision at a single instance in time and longitudinal space direction, indeed. In a coordinate system consisting of the longitudinal proper time $\tau = \sqrt{t^2 - z^2}$, the transverse coordinates x, y, and rapidity $\eta = \mathrm{arctanh}(z/t)$, the fluid velocity is of the form $u^\mu = (u^\tau, u^x, u^y, 0)$, i. e. the fluid velocity in the rapidity direction vanishes. If scalar functions like energy density depend on t and z only in terms of the proper time, $\epsilon = \epsilon(\tau, x, y)$ an invariance under boosts in the longitudinal direction $\eta \to \eta + \Delta\eta$ arises (so called Bjorken boost invariance). The remaining initial value problem to be solved is then effectively only 2+1 dimensional. This is a substantial simplification. Bjorken boost symmetry is an idealization but it is reasonably accurate close to mid-rapidity $\eta \approx 0$.

Based on the above considerations one can construct a toy model that can almost be solved analytically. Consider initial conditions at $\tau = \tau_0$ of the form $\epsilon = \epsilon(\tau_0)$, $u^\mu = (1, 0, 0, 0)$. This describes an initial energy density that is extended over the whole transverse plane. Although this is of course not realistic for the whole fireball it constitutes a simplified model for inner region at early times after a central collision. In addition to Bjorken boost invariance $\eta \to \eta + \Delta\eta$, the initial conditions are now also symmetric with respect to translations and rotations in the transverse plane. Together, these symmetries imply that $u^\mu = (1, 0, 0, 0)$ for all times τ and that $\epsilon = \epsilon(\tau)$ is independent of x, y and η. It remains to solve a single, 0+1 dimensional differential equation to determine $\epsilon(\tau)$. In the first order formalism of viscous relativistic fluid dynamics, this equation reads

$$\partial_\tau \epsilon + (\epsilon + p)\frac{1}{\tau} - \left(\tfrac{4}{3}\eta + \zeta\right)\frac{1}{\tau^2} = 0. \tag{18}$$

The solution depends on the thermodynamic equation of state $p(\epsilon)$ and the viscosities $\eta(\epsilon)$ and $\zeta(\epsilon)$.

For example, assuming $p \sim \epsilon \sim T^4$ leads to

$$\partial_\tau T + \frac{T}{3\tau}\left(1 - \frac{4\eta/3 + \zeta}{sT\tau}\right) = 0. \tag{19}$$

The solution for $\eta/s = \text{const}$ and $\zeta = 0$ is

$$T(\tau) = T(\tau_0)\left(\frac{\tau_0}{\tau}\right)^{1/3}\left[1 + \frac{2}{3\tau_0 T(\tau_0)}\frac{\eta}{s}\left(1 - \left(\frac{\tau_0}{\tau}\right)^{2/3}\right)\right]. \tag{20}$$

For an ideal fluid where $\eta/s = 0$, or more general at late times, the temperature simply decays like $T \sim \tau^{-1/3}$. This is due to the dilution of the fluid by the longitudinal expansion. For $\eta/s > 0$ and at early times there is in addition a small heating effect due to shear viscosity. Fig. 5 illustrates the solution in eq. (20) for different values of η/s.

Let us now increase the level of complexity by one step and study an initial energy density with somewhat more realistic dependence on the transverse coordinates. For an azimuthally symmetric, central collision event, the energy density is of the form $\epsilon = \epsilon(\tau, r)$ where $r = \sqrt{x^2 + y^2}$. Connected with the initial energy distribution is a pressure gradient in radial direction which leads after a short time to a positive fluid velocity in radial direction, $u^r > 0$, the so-called radial flow. To determine $\epsilon(\tau, r)$ or $T(\tau, r)$ and the fluid velocity $u^r(\tau, r)$ one needs so solve a system of 1+1 dimensional, coupled differential equations, which is still rather easy to do numerically. A solution for $T(\tau, r)$ obtained for a realistic initial temperature profile, as well as equation of state and viscosities, is shown in Fig. 6. The effects of the longitudinal as well as radial expansion are clearly visible.

Before we continue our endeavor of solving viscous relativistic fluid dynamics for more and more realistic initial conditions, let us pause for a moment and consider the process of kinetic freeze-out.

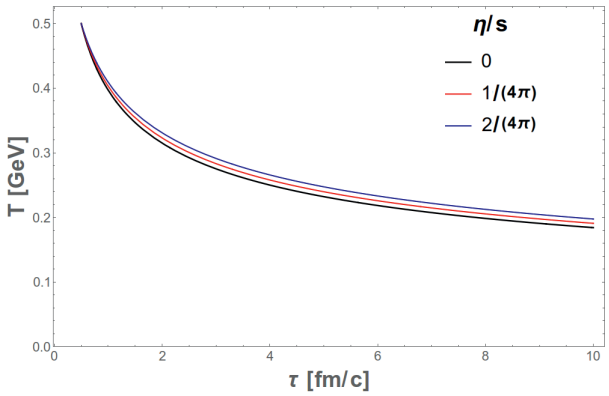

Fig. 5: Bjorken flow solution for temperature T as a function of proper time τ for different values of the ratio of shear viscosity to entropy density η/s. Figure taken from ref. [24].

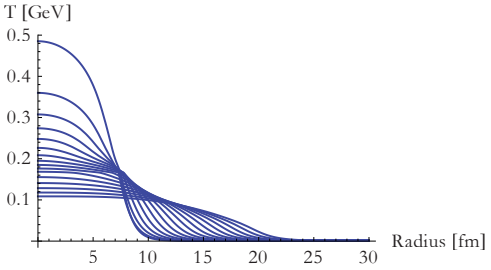

Fig. 6: Temperature profile $T(\tau, r)$ as a function of radius r for different times τ. The equation of state, shear viscosity and initial values are chosen as described in ref. [25].

Although we can in principle follow the dynamics of the expansion and the associated dilution and cool-down of the fluid as described by fluid dynamics down to very small temperatures, there is in reality a point where the fluid dynamic description breaks down. Indeed, after the transition from quarks and gluons to hadronic degrees of freedom and when the temperature and densities drop further, collisions become less and less frequent. At some point, hadrons stop interacting and occupation numbers in momentum space do not change any more. This is the process of kinetic freeze-out.

Just before the freeze-out one might assume local close-to-equilibrium occupation numbers of hadrons in each fluid element

$$\frac{dN_i}{d^3p d^3x} = f_i(p^\mu; T(x), u^\mu(x), \pi^{\mu\nu}(x), \pi_{\text{bulk}}(x)). \tag{21}$$

The occupation numbers for each particle species as a function of the thermodynamic variables, the fluid velocity and the dissipative shear stress and bulk viscous pressure can in principle be determined from microscopic calculations. For example, neglecting the effect of $\pi^{\mu\nu}$ and π_{bulk} and assuming an ideal gas with Boltzmann statistics gives

$$f_i = c_i \, e^{\frac{u_\mu(x) p^\mu}{T(x)}} \to c_i \, e^{-\frac{E_{\vec{p}} - \vec{v}(x)\cdot\vec{p}}{T(x)}} \quad (\vec{v}^2 \ll c^2). \tag{22}$$

In the last expression we have taken the non-relativistic limit for illustration. The factor c_i accounts for the degeneracy due to spin. Summing up the contribution of all fluid cells in terms of an integral over the three-dimensional freeze-out hyper-surface (or hyper-surface of last scattering) Σ_f yields particle spectra in momentum space as they can actually be measured in the particle detector [26],

$$E\frac{dN_i}{d^3p} = -\frac{1}{(2\pi)^3} p^\mu \int_{\Sigma_f} d\Sigma_\mu \, f_i. \tag{23}$$

The freeze-out surface is in principle determined by the dynamics of expansion and the scattering processes. In practice it is often assumed for simplicity that is corresponds to a surface of constant temperature $T_{\rm fo}$ in the region around 100 MeV.

The particle spectra $E\frac{dN_i}{d^3p}$ are usually written in terms of the momentum rapidity $y = \text{arctanh}(p^z/E)$, the transverse momentum p_T and the momentum azimuthal angle ϕ as $dN_i/(dyd\phi\ p_T dp_T)$. They inherit some symmetry properties from the fluid dynamic fields. For example, when the fluid dynamic fields are independent of position-space rapidity η, the spectrum is independent of momentum space rapidity y. Similarly, the spectrum originating from an azimuthally symmetric solution of fluid dynamics is independent of the momentum-space azimuthal angle ϕ.

In order to reliably calculate the particle spectrum $dN_i/(dyd\phi\ p_T dp_T)$ one has to solve the relativistic fluid dynamic equations. There is, however, also a shortcut that is often used to study some aspects of the resulting particle spectrum, the so-called blast-wave models. For these, the particle spectra are not determined from realistic solutions of fluid dynamics but rather for a simplified ansatz and a simple parametrization of the kinetic freeze-out surface. For example, one might assume for simplicity that freeze-out takes place at constant time τ_f and in a transverse area with radius $r < r_{\rm max}$. If one also assumes constant temperature T and radial flow velocity v_r, as well as the Boltzmann occupation numbers as in equation (22), one can solve the integrals in eq. (23) and one obtains the analytic expression

$$\frac{dN_i}{dyd^2p_T} = \frac{c_i}{4\pi^2}\tau_f r_{\rm max}^2 \sqrt{p_T^2+m_i^2}\ K_1\left(\frac{\sqrt{p_T^2+m_i^2}}{T\sqrt{1-v_r^2}}\right) I_0\left(\frac{p_T v_r}{T\sqrt{1-v_r^2}}\right), \tag{24}$$

where $K_1(\cdot)$ and $I_0(\cdot)$ are Bessel functions. Many variants of such simple blast-wave models have been studied. They capture some qualitative features of full fluid dynamics solutions. Generically, particle spectra following from integrals over thermal occupation numbers are close to exponential shape. The radial flow velocity, so-called radial flow, leads to a "blue shift" of the particle spectrum. Another generic observation is that particle spectra become steeper for smaller particle mass m_i.

An experimental result for the spectrum of charged particle as a function of p_T is shown in Fig. 7. For the 0-5% most central collisions and small p_T, the spectrum has an almost exponential form indeed, with the slope determined by freeze-out temperature and radial flow velocity. In contrast, for peripheral collisions, the spectrum measured in heavy ion collisions is of a form similar to the proton-proton reference.

Let us now come to non-central collisions. The overlap region of two nuclei, illustrated in Fig. 8, is approximately "almond shaped". Correspondingly, the initial energy density at the point where a fluid dynamic description becomes valid, has this shape, as well. The pressure gradients are larger in the reaction plane which leads after some time of fluid dynamic evolution to a larger fluid velocity in this direction. The freeze-out formula in eq. (23) implies then that more particles fly in this direction after freeze-out than in the transverse direction orthogonal to this. This asymmetry is quantified in terms of the elliptic flow coefficient v_2.

Quite general, an azimuthal particle distribution can be expanded like

$$\frac{dN}{d\phi} = \frac{N}{2\pi}\left[1 + 2\sum_m\ v_m\ \cos\left(m\left(\phi-\psi_m\right)\right)\right] \tag{25}$$

where the coefficients v_m are called harmonic flow coefficients and the ψ_m are corresponding angles (obviously the ψ_m are defined modulo $2\pi/m$). If the particle asymmetry originates solely from the orientation of the reaction plane, the angles should all be the same, $\psi_m = \psi_R$ (up to terms π/m which determine the sign of v_m). Moreover, the symmetry with respect to $\phi \to \phi + \pi$ of the configuration in Fig. 8 would imply $v_1 = v_3 = v_5 = \ldots = 0$.

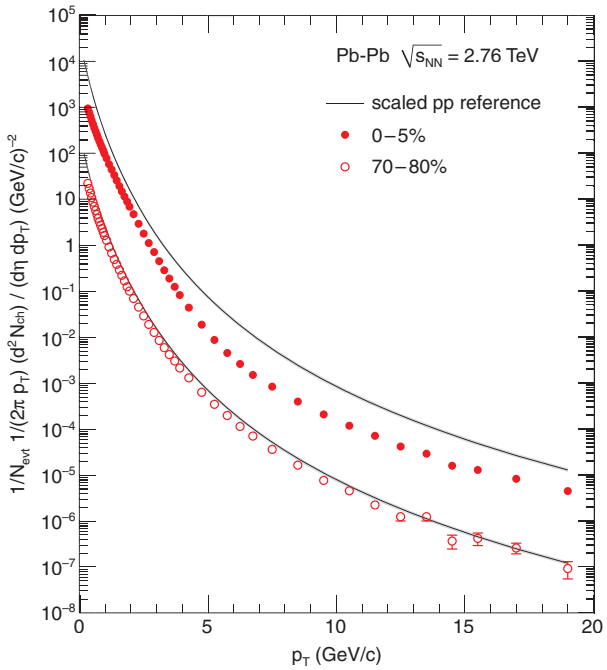

Fig. 7: Charged particle spectrum as a function of the transverse momentum in central (0 - 5%) and peripheral (70 - 80%) heavy ion collisions as measured by the ALICE collaboration. Figure taken from ref. [27].

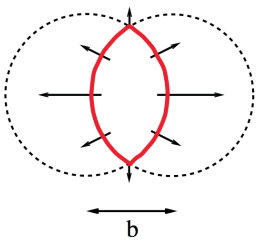

Fig. 8: Illustration of a non-central heavy ion collision. The dashed lines mark the density of the two colliding nuclei in the transverse plane, the red line marks the overlap region. The arrows illustrate the elliptic flow which results from the initial pressure gradients. Figure taken from ref. [2].

At this point, some remarks on experimental techniques are in order. The impact parameter of a heavy ion collisions is of course random. It can neither be adjusted nor be measured precisely. There is, however, a statistical method to say something about impact parameters. The underlying principle is that very central collisions produce more charged particles, in contrast to more peripheral collisions. One can order the full set of events recorded during some measurement campaign according to the multiplicity and divide them into classes - so called centrality classes. An histogram-type diagram with the corresponding centrality classes is shown in Fig. 9. Using further elements of modeling - for example based on the so-called Glauber model - one can associate impact parameters, or ranges of impact parameters, to these centrality classes with the highest multiplicity class corresponding to the smallest impact parameters. The harmonic flow coefficients v_m can also be measured as a function of transverse momentum p_T. An example for elliptic flow is shown in Fig. 10 for different centrality classes in a comparison between early results from the LHC and similar measurements at RHIC.

A very interesting observables is also a two-particle correlation function defined by a ratio of the expectation value of particle distributions at two angles ϕ_1 and ϕ_2 by two separate expectation values of

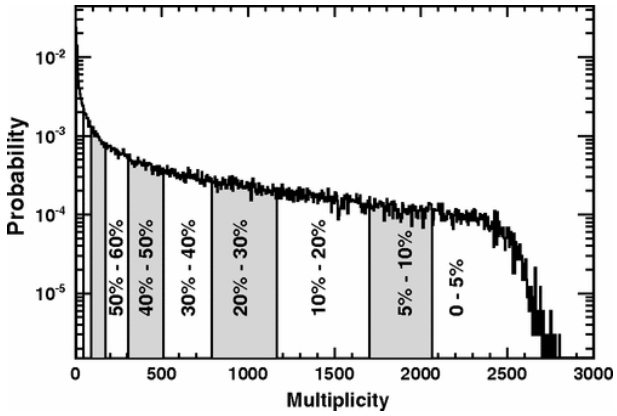

Fig. 9: Centrality classes as determined via the multiplicity in the Time Projection Chamber (TPC) by the ALICE collaboration. Figure taken from ref. [28].

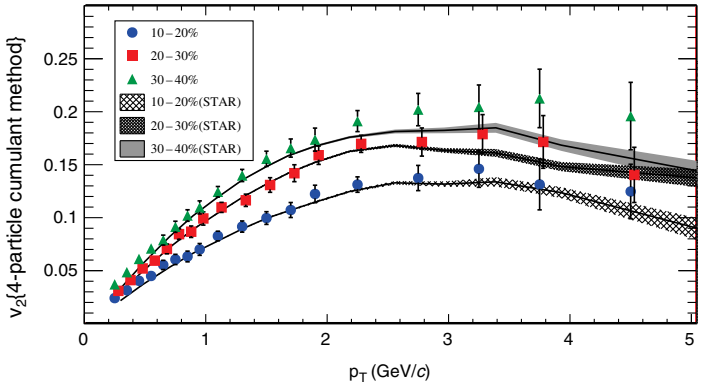

Fig. 10: Elliptic flow v_2 as a function of transverse momentum for different centrality classes as measured by the ALICE collaboration at the LHC (symbols) and by the STAR collaboration at RHIC (shaded regions). Figure taken from ref. [28].

this type,

$$C(\phi_1,\phi_2) = \frac{\langle \frac{dN}{d\phi_1}\frac{dN}{d\phi_2}\rangle_{\text{events}}}{\langle \frac{dN}{d\phi_1}\rangle_{\text{events}}\langle \frac{dN}{d\phi_2}\rangle_{\text{events}}} = 1 + 2\sum_m v_m^2 \cos(m\,(\phi_1-\phi_2)). \tag{26}$$

A priori, this depends on the two angles ϕ_1 and ϕ_2 but due to the statistical azimuthal rotation symmetry it is a function of the difference $\phi_1 - \phi_2$, only. Experimentally, the correlation function is typically measured with a rapidity gap $\Delta\eta$ imposed between the two particles whose correlation in azimuthal angle is studied. The last equation in (26) is the prediction for this correlation function in a fluid dynamic model. It shows that one can obtain the squares of the harmonic flow coefficients v_m^2 by performing a Fourier decomposition of the correlation function $C(\phi_1 - \phi_2)$. Now, surprisingly, if one does the corresponding analysis for a set of events with very high multiplicity corresponding to the centrality class with the lowest impact parameters as shown in Fig. 11, one finds that the flow coefficients v_2, v_3, v_4, v_5 and v_6 are actually all non-zero! At the same time, the full correlation function is actually very nicely represented by the superposition of these harmonic modes.

This result is surprising for two reasons. First, the symmetry with respect to $\phi \to \phi + \pi$ discussed below eq. (25) would imply that the odd flow coefficients v_3, v_5 etc. should vanish. Moreover, for very central collisions, the elliptic flow coefficient v_2 as well as higher order even coefficients v_4, v_6 etc. should actually vanish, as well, if they simply measure the effect of a non-vanishing impact parameter. The fact that this is not the case shows that additional effects not discussed so far must play a role here.

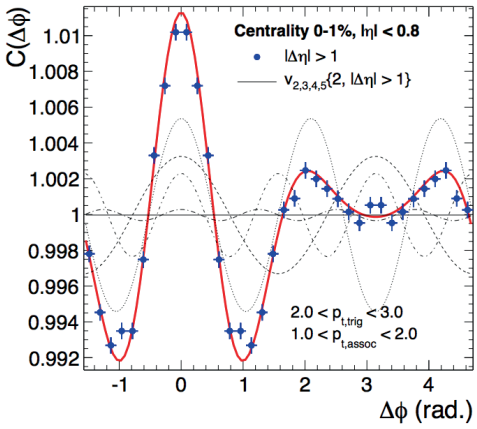

Fig. 11: Two-particle azimuthal correlation for the 0-1% centrality class as measured by the ALICE collaboration. The solid red line shows the sum of the contributions from anisotropic flow coefficients v_2, v_3, v_4 and v_5 (dashed lines). Figure taken from ref. [30].

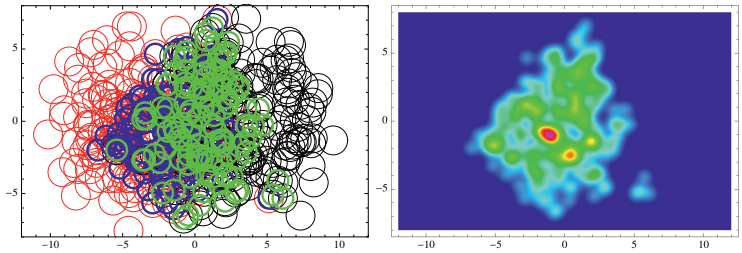

Fig. 12: Transverse energy density from a Monte-Carlo Glauber model. See text for further explanations. Figure taken from ref. [31].

In fact, what we have not discussed so far, are event-by-event fluctuations in the initial energy density distribution. We have based our arguments, for example for $v_3 = v_5 = 0$, on smooth and symmetric energy densities corresponding to expectation values. For a single event, the energy densities can deviate from this simple picture, however. This is actually predicted by realistic models of the initial state. Consider for example the Glauber model. The nuclei are here modeled as a combination of nucleons which have a statistical distribution in the form of a Woods-Saxon profile. A heavy ion collision is modeled by a superposition of individual collisions between nucleons. We will not discuss the details of this model here but illustrate the resulting energy density in Fig. 12. On the left hand side, the transverse positions of the nucleons in the two nuclei are marked by the red and black rings. The size corresponds to the nuclear cross section. Those nucleons that overlap with nucleons from the other nucleus are marked in addition by blue and green rings. The right hand side of fig. 12 shows the energy density that results if one associates a certain Gaussian-shaped contribution to each individual nucleon-nucleon collision.

Because of the fluctuations in the initial energy density, sizable flow coefficients v_m can be generated by the fluid dynamic expansion, even for central collisions. Beyond the energy density, also the other fluid dynamic fields such as fluid velocity, shear stress, bulk viscous pressure or baryon number density may actually have fluctuating initial configurations. It is currently an interesting direction of research to understand this better, both from analyzing experimental data and from theoretical investigations.

At this point, a few remarks on theoretical simulations of heavy ion collisions based on relativistic fluid dynamics might be in order. Specialized numerical codes have been developed for this purpose and typically they solve a variant of second order relativistic fluid dynamics for given initial conditions

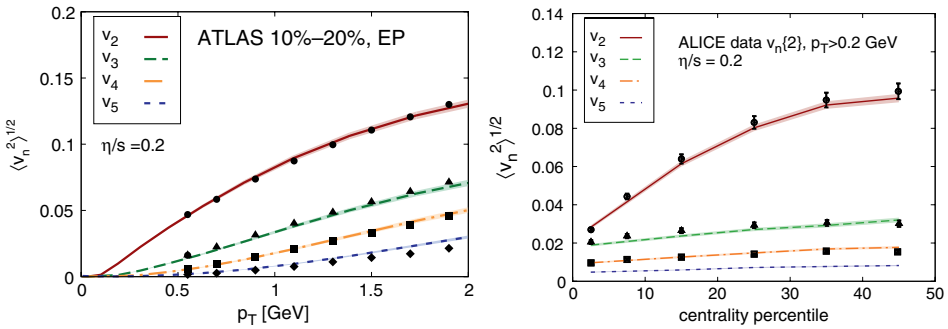

Fig. 13: Root-mean-square anisotropic flow coefficients $\langle v_n^2 \rangle^{1/2}$ as a function of transverse momentum (left panel) and centrality (right panel) as calculated by numerical fluid dynamic simulations [32], compared to experimental data by the ATLAS [29] and ALICE collaborations [30]. Figures taken from ref. [32].

and also include a description of the kinetic freeze-out and in some cases a subsequent phase of hadron resonance decays and further scatterings described by kinetic theory. The codes use the thermodynamic equation of state as calculated from lattice QCD and initial conditions which fluctuate from event-to-event and are calculated from the Monte-Carlo Glauber or related models. The transport properties such as η/s are usually varied with the goal of determining the experimentally favored value. A result of such a comparison is shown exemplarily in Fig. 13. Typical values for η/s that are favored by such comparisons between theory and experiment are in the range of a few times $1/(4\pi) \approx 0.08$. This suggests that the fluid dynamics in the relevant phase might be dominated by strongly coupled degrees of freedom. More realistically, η/s should not be constant but vary with temperature T and it will be one of the challenges for the coming years to see how one can constrain this dependence from the experimental data.

6 Initial state fluctuations and their fluid dynamic propagation

Because fluctuations in fluid dynamic fields have played such an interesting role in heavy ion phenomenology in the recent years, and will probably continue to do so in the coming years, we will discuss them here in a little more detail.

Interesting are in particular initial fluid perturbations which are event-by-event fluctuations around a background or average of fluid fields at the (proper) time τ_0 where the fluid dynamic description is initialized. Examples for fluid dynamic fields are the energy density ϵ, the fluid velocity u^μ, the shear stress $\pi^{\mu\nu}$ or the bulk viscous pressure $\pi_{\rm bulk}$. Although they can usually be neglected, there are questions for which also other variables like the baryon number density n_B, the electric charge density, electromagnetic fields or others have to be taken into account. Fluctuations in fluid fields are particularly interesting because they are governed by universal evolution equations and because they can be used to constrain the thermodynamic and transport properties of a QCD fluid. Moreover, they contain interesting information from early times and can be taken as a measure for deviations from complete thermal equilibrium.

In some respects, the situations is similar as for the cosmic microwave background and the large scale structure which are studied in cosmology. Also there, the fluctuation spectrum contains very interesting information from early times and from the history of the dynamical expansion. Much can be learned because many numbers can be measured and compared to theory. This in turn has lead cosmologists to a detailed understanding of the evolution history and the properties of our universe. A similar development may eventually trigger something like a precision era in heavy ion physics.

What would one have to do to understand initial fluid fluctuations in detail? Here is a program: First, one would have to characterize initial state fluctuations in a suitable and ideally complete way. Second, these fluctuations or perturbations need to be propagated through the fluid dynamic regime. Third, one has to determine their influence on particle spectra and harmonic flow coefficients. Finally,

one should take also perturbations from non-hydro sources, as for example jets, into account.

One possibility to implement the above program is in terms of numerical simulations, or more specific, event-by-event viscous relativistic hydrodynamic simulations (see e.g. ref. [33] for a recent overview). However, one can also make progress by (semi) analytic methods which are closer to the theoretical methods used to in cosmology. This shows the parallels between the big bang and the little bangs in the laboratory in more detail.

The theoretical approach called "Mode-by-mode fluid dynamics" or "Fluid dynamic perturbation theory for heavy ions" works in analogy to the Cosmological perturbation theory [25]. For that, one first solves the fluid equations of motion for a smooth background corresponding essentially to an averaged initial condition and afterwards order-by-order in perturbations around that configuration. The convergence properties of this expansion have been investigated and seem favorable [34]. The background solution can be taken symmetric with respect to azimuthal rotations and Bjorken boosts in the longitudinal direction while the perturbations can break these (statistical) symmetries.

For mode-by-mode fluid dynamics, a characterization of initial conditions in terms of a Bessel-Fourier expansion is particularly favorable. To that end one writes a transverse density distribution, say for the enthalpy density $w = \epsilon + p$ in the following form [25, 35, 36],

$$w(r,\phi) = w_{\rm BG}(r) + w_{\rm BG}(r) \sum_{m,l} w_l^{(m)}\, e^{im\phi}\, J_m\left(z_l^{(m)} \rho(r)\right). \tag{27}$$

The function $w_{\rm BG}(r)$ parametrizes the azimuthally symmetric background configuration. The argument of the Bessel functions J_m is given by the numbers $z_l^{(m)}$ which correspond to the l'th zero crossing of the function $J_m(z)$, and the function $\rho(r)$ which maps the relevant range of transverse radii r to the interval [0,1]. A particularly useful choice is discussed in ref. [36].

The expansion coefficients $w_l^{(m)}$ are dimensionless and have a discrete azimuthal wavenumber m as well as a radial wavenumber l. Higher values of m and l correspond to finer spatial resolution. The coefficients $w_l^{(m)}$ can also be related to the so-called eccentricities, another popular way to characterize initial transverse density distributions. While the expansion in (27) can be used for scalar quantities such as enthalpy density, a similar expansion can be used for vectors (such as the fluid velocity) and tensors (such as the shear stress). Observe that when all the coefficients $w_l^{(m)}$ vanish, one is left with the background configuration, only. The configuration in (27) is independent or rapidity η but it is straight forward to extend the scheme in that direction.

Quite generically, one can now solve the fluid equations of motion by the following perturbative scheme. One writes the hydrodynamic fields $h = (w, u^\mu, \pi^{\mu\nu}, \pi_{\rm Bulk}, \ldots)$ at initial time τ_0 as $h = h_0 + \epsilon\, h_1$ with the background configuration h_0 and the fluctuation part $\epsilon\, h_1$. We have introduced here a formal expansion parameter ϵ. At later times $\tau > \tau_0$ one can write the fluid fields as $h = h_0 + \epsilon\, h_1 + \epsilon^2 h_2 + \epsilon^3 h_3 + \ldots$. Solving for the time evolution in this scheme implies to determine h_0 as the solution of full, non-linear fluid equations but in a partcularly symmetric situation with azimuthal rotation and Bjorken boost invariance. The linear term h_1 is a solution of the linearized fluid equations where the linearization is done around the background configuration h_0. This solution can be determined mode-by-mode, i. e. for each mode with one azimuthal wavenumber m and radial wavenumber l in the expansion (27). The quadratic term h_2 can be obtained from an iterative solution involving quadratic interactions between modes and so on.

In order to find the linear solution h_1, it is advantageous to use again a Fourier expansion in the azimuthal direction and with respect to rapidity. In that way, one can effectively reduce the numerical problem from a 3+1 dimensional partial differential equation to a 1+1 dimensional one. The latter is rather easy to solve numerically. This reduction of the complexity helps also to find the quadratic and higher order terms.

The perturbative scheme can also be used at freeze-out. For that purpose one propagates both

the background and the perturbations until the freeze-out surface has been reached. In the perturbative scheme, the latter is determined by the background solution alone and can correspond for example to constant background temperature. (In general, there is no precise understanding of where the freeze-out surface is positioned exactly.) The freeze-out surface is then as symmetric as the background configuration. Also the particle spectrum due to the background inherits these symmetries. However, the corrections due to the perturbations are not symmetric. In contrast, at linear order, they inherit the transformation behavior of the initial modes. At quadratic and higher orders this is a little more involved but straight forward to determine directly or by simple group theoretic methods.

One can expand the resulting particle spectrum for a single event to linear order in initial state perturbations like [37]

$$\ln\left(\frac{dN^{\text{single event}}}{p_T dp_T d\phi dy}\right) = \underbrace{\ln S_0(p_T)}_{\text{from background}} + \underbrace{\sum_{m,l} w_l^{(m)} e^{im\phi}\theta_l^{(m)}(p_T)}_{\text{from fluctuations}} + \dots . \tag{28}$$

Note that each mode comes with an angle, $w_l^{(m)} = |w_l^{(m)}|\, e^{-im\psi_l^{(m)}}$ and the contribution of each mode has different p_T-dependence, $\theta_l^{(m)}(p_T)$. At quadratic order, the expression in (28) is supplemented by a term or the form

$$\sum_{m_1,m_2,l_1,l_2} w_{l_1}^{(m_1)} w_{l_2}^{(m_2)}\; e^{i(m_1+m_2)\phi}\, \kappa_{l_1,l_2}^{(m_1,m_2)}(p_T). \tag{29}$$

The non-linearities parametrized by the function $\kappa_{l_1,l_2}^{(m_1,m_2)}(p_T)$ arise both from the non-linear terms in the fluid dynamic evolution and from non-linear terms at freeze-out.

One can also determine the harmonic flow coefficients defined in eq. (25) within this scheme. For a single event one has

$$\begin{aligned} V_m^* &= v_m e^{-i\,m\,\psi_m} \\ &= \sum_l S_{(m)l}\, w_l^{(m)} + \sum_{\substack{m_1,m_2,\\ l_1,l_2}} S_{(m_1,m_2)l_1,l_2}\, w_{l_1}^{(m_1)}\, w_{l_2}^{(m_2)}\, \delta_{m,m_1+m_2} + \dots \end{aligned}$$

The function $S_{(m)l}$ is here the linear dynamic response function and $S_{(m_1,m_2)l_1,l_2}$ may be called a quadratic dynamic response function and so on. The symmetries of the problem imply a conservation of azimuthal wavenumber. The response functions can be determined and they depend on the thermodynamic and transport properties of the fluid formed by the quark gluon plasma, in particular viscosity. One of the challenges for the coming years will be to understand these dependencies in detail and to use the experimental knowledge about the response functions in order to constrain the thermodynamic and transport properties of QCD from experimental data.

7 Jet quenching

We will now leave the fluid dynamic considerations aside and concentrate for the remaining time on processes at higher energies. More specific, consider again the transverse momentum distribution of charged particles in Fig. 7. At small transverse momenta and for central collisions, the particle spectra are determined by the decay products of a thermalized medium. This is reflected in a close-to-exponential shape, which shows up as a straight line on the logarithmic scale of Fig. 7. In contract, the physics of high energetic particles and partons is different: they are not thermalized but can nevertheless be influenced by the medium. More specific, they can loose energy and momentum to the medium when they fly through it.

To understand this in a little more detail, let us first recapitulate some elements of the description of high energetic processes in conventional hadron collisions (for example proton - proton or proton -

antiproton collisions). An important theoretical concept is the one of *factorization*. According to this principle, processes at high energy are governed by a convolution of

- Process-independent *parton distribution functions* which parametrize the probability to find partons with given momentum in the incident hadron.
- Process-dependent *hard scattering cross sections* which determine the probability that initial partons scatter to final state partons with given momenta.
- Process-independent *parton fragmentation functions* which describe the probability that final state partons fragments into a jet with certain hadron content.

A very detailed theoretical and experimental understanding of high energetic processes in hadron collisions using perturbative QCD has been gained over the years with the help of the factorization principle. This constitutes a solid foundation to measure changes occurring in heavy ion collisions. A very short summary of these changes is as follows. Nuclear parton distribution functions differ from proton parton distribution functions but may be measured by proton-nucleus collisions, electron-nucleus collisions etc. Hard scattering cross sections are not modified by the medium if the momentum transfer is high enough. The key modification in a heavy ion context compared to hadron collisions is: After production, high energetic partons must propagate through the hot and dense medium produced in heavy ion collisions. By interactions with the (soft) gluons and quarks in the medium, high energetic partons loose part of their energy and momentum. Because parton production rates are steeply falling with energy, energy loss leads to a reduction of the number of partons with large energy. This can be clearly seen in Fig. 7.

The energy loss of highly energetic partons in a heavy ion collision can also be seen on the level of reconstructed jets. One prominent observable in this context is the so-called dijet asymmetry which is defined as

$$A_J = \frac{p_{T,1} - p_{T,2}}{p_{T,1} + p_{T,2}} \tag{30}$$

where $p_{T,1}$ and $p_{T,2}$ are the transverse momenta of a leading and a sub-leading jet, respectively. Event distributions of this observable are shown in Fig. 14 for different centrality classes, as measured by the CMS collaboration. Also shown there are results of simulations based on the Monte-Carlo code PYTHIA, which does not take any jet energy loss into account. For peripheral collisions, the distribution is also compared to proton-proton collisions. As one can see clearly, the measured asymmetries in heavy ion collisions have the tendency to be larger than in the simulations for central collisions, which illustrates that a significant fraction of transverse momentum gets transported outside the jet cone by interactions with the medium.

We do not have the space here to discuss the theory of jet energy loss in detail. Very briefly, the main parton energy loss mechanism in QCD is medium induced gluon radiation [39, 40]. This is in some aspects analogous to bremsstrahlung in QED. While in vacuum QCD, there are essentially only small angle (colinear) splittings of gluons and quarks, in the context of a heavy ion collisions, additional kicks from scattering with the medium lead to larger angles. In a statistical description, this leads to a broadening of the transverse momentum $k_\perp$ (orthogonal to the main parton momentum) by a diffusion or random walk type process,

$$\frac{d}{dt}\left\langle k_\perp^2 \right\rangle = \hat{q}. \tag{31}$$

Here, $\hat{q}$ is the so-called jet quenching parameter. Based on this principle, a detailed theoretical description can be formulated. In addition to transverse momentum broadening, interactions with the medium also induce color decoherence. Jet energy loss models have been implemented also in Monte-Carlo codes, for example JEWEL [41, 42].

In addition to calorimetric jet observables, a traditional measure of energy loss is the so called

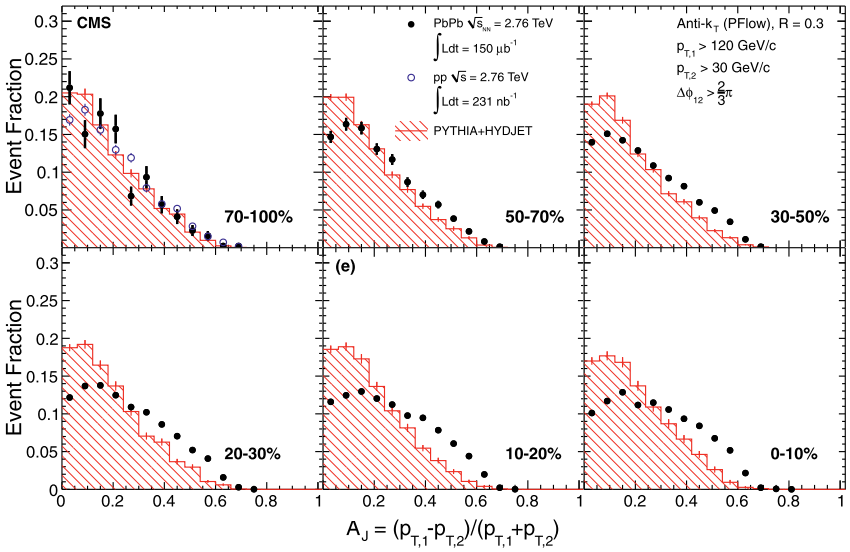

Fig. 14: Dijet asymmetry ratio A_J for leading jets of $p_{T,1} > 120$ GeV and sub-leading jets of $p_{T,2} > 30$ GeV, with a selection of $\Delta\phi_{1,2} > 2\pi/3$ between the two jets, for different centrality classes. Experimental results (points) are compared to simulations (histograms) based on PYTHIA and HYDJET (without any parton energy loss). Figure taken from ref. [38].

nuclear modification factor,

$$R^h_{AA}(p_T, \eta, \text{centrality}) = \frac{\frac{dN^{AA\to h}_{\text{medium}}}{dp_T d\eta}}{\left\langle N^{AA}_{\text{coll}} \right\rangle \frac{dN^{pp\to h}_{\text{vacuum}}}{dp_T d\eta}}. \tag{32}$$

This ratio of production cross sections for a particle h in heavy ion (AA) collisions and the scaled proton-proton (pp) reference can be defined for many different processes. It depends in general on transverse momentum p_T, rapidity η and centrality but some of these variables are sometimes integrated over. Nuclear modification factors have been measured for many different particles h. Note that this variable depends also sensitively on the proton-proton reference. This can sometimes be a problem, in particular when no measurements exist for a given collision energy and one therefore has to rely on interpolations. In a similar way to R_{AA}, one defines also the modification factor R_{pA} for proton - ion collisions or R_{CP} as a ratio between cross sections for central and peripheral collisions.

A compilation of various nuclear modification factors by the CMS collaboration is shown in Fig. 15. One observes that unidentified charged particles and b-quarks are quenched, while photons, W- and Z-bosons are not quenched, i.e. they have $R_{AA} = 1$ within the experimental uncertainties. This is of course expected because these particles are color-neutral.

8 Quarkonia in hot matter

For the last part of these introductory lectures we will be concerned with quarkonia, which are bound states of heavy quark - antiquark pairs in the context of heavy ion collisions. This is a traditional field of study in the context of the quark gluon plasma for the following reasons.

Some interesting and important questions concerning the quark gluon plasma are: How can one test deconfinement of quarks and gluons at large temperature? Or related: What prevents the formation of a meson in a quark-gluon plasma? The attractive force between a quark and an antiquark is actually screened within a plasma at non-vanishing temperature when the two are separated by more than the typical distance between free color charges in the medium. This effect can be seen nicely in lattice QCD

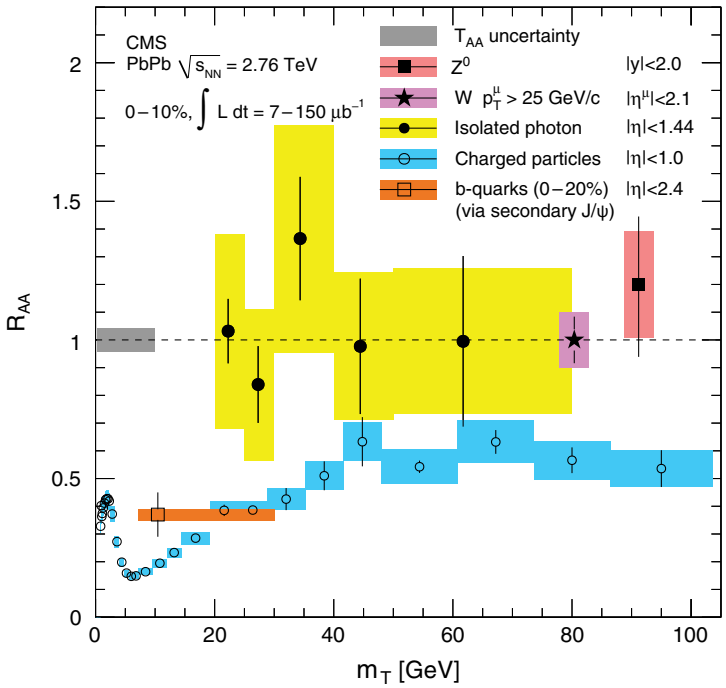

Fig. 15: Nuclear modification factor R_{AA} for different particles as a function of the transverse mass $m_T = \sqrt{m^2 + p_T^2}$ as measured and compiled by the CMS collaboration. Figure taken from ref. [43].

simulations.

One can ask more quantitatively: How close do quark and anti-quark have to be in order for their interaction not to be screened? And how does this depend on temperature? It was suggested to investigate these questions for bound states of heavy quark-antiquark pairs (quarkonia) by Matsui and Satz in 1986 [44].

A few examples of charmonium states ($c\bar{c}$ bound states) are the J/ψ(1S) with a mass of 3.09 GeV, the ψ(2S) with a mass of 3.69 GeV, the χ_{c1}(1P) with mass 3.51 GeV or the χ_{c2}(1P) with a mass of 3.56 GeV. Some bottomonium states ($b\bar{b}$ bound states) are the $\Upsilon(1S)$ with mass 9.46 GeV and its excited states, the $\Upsilon(2S)$ with a mass of 10.02 GeV and the $\Upsilon(3S)$ with a mass of 10.36 GeV.

The traditional picture of what should happen to these bound states at non-vanishing temperature is the one of sequential suppression. Qualitatively, when the temperature is increased, larger mesons or bound states are hindered from binding first while smaller bound states can survive up to higher temperature. (The typical distance between free color charges becomes smaller at higher temperature.) An heuristic Schrödinger equation approach using screened static quark potentials [45] suggests for example that the J/ψ(1S) dissociates at $T_d \approx 2.1\,T_c$. The $\psi(2S)$ is larger and dissociates at $T_d \approx 1.1\,T_c$. The bottomonium state $\Upsilon(1S)$ dissociates at $T_d \approx 4\,T_c$ while $\Upsilon(2S)$ is larger and dissociates already at $T_d \approx 1.6\,T_c$ and $\Upsilon(3S)$ is even larger and dissociates at $T_d \approx 1.2\,T_c$. While this picture gives some guidance, the use of static potentials to describe bound states in a QCD medium is somewhat questionable.

While there is little doubt that the qualitative picture sketched above is qualitatively correct, there are also some confounding effects that must be taken into account to properly understand quarkonia in the context of heavy ion collisions. Some of them are:

- Cold nuclear matter effects (which are already present for pA collisions) must be understood.
- The collective dynamics of heavy ion collisions plays a role, i. e. the expansion, fluid dynamic flow etc.

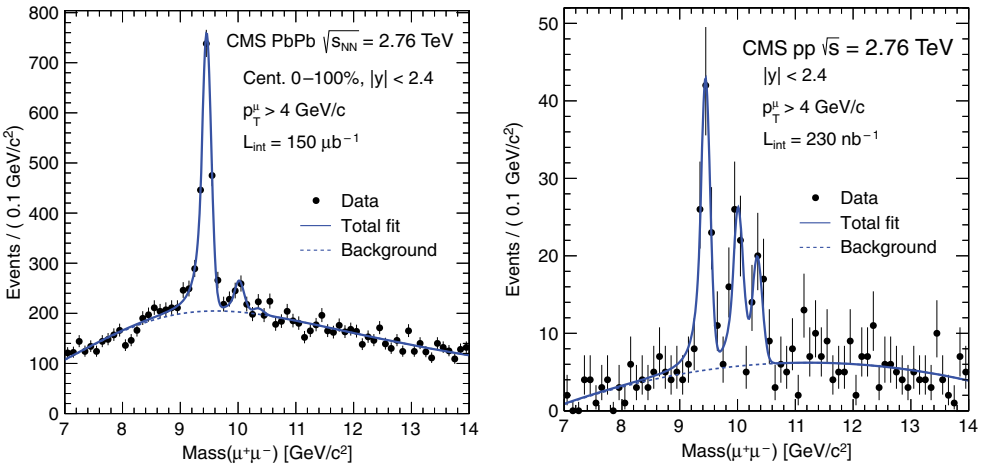

Fig. 16: Invariant mass spectrum of di-muons in heavy ion (left panel) and proton-proton (right panel) collisions. See text for further discussion. Figures taken from ref. [46].

- Quarkonia are in general not at rest with respect to the medium.
- The formation of quarkonium bound states is purely understood but should also takes some time. What is the influence of the medium for that process?
- Quarkonia can also be formed by recombination of open heavy quarks at hadronization / chemical freeze-out.

At present there is no clear picture about the quantitative importance and the interplay of all these effects, yet. However, experimental and theoretical efforts to improve the understanding of quarkonia in the context of heavy ion collisions are ongoing.

As a particularly clear example for the suppression effects that can arise due to a hot medium, consider the number of $\mu^+ \mu^-$ pairs as a function of their center of mass energy as measured by CMS. Fig. 16 shows this for Pb-Pb collisions in the left panel and for comparison the corresponding curve for proton-proton collisions in the right panel. One can see directly that the excited states of Υ are clearly suppressed in heavy ion collisions compared to pp collisions at the equivalent collision energy. It is a more difficult question, however, whether this already proves sequential suppression according to the Matsui & Satz picture.

9 Conclusions

To conclude these introductory lectures one may say that we are on the way of understanding the properties of QCD at high temperature and density with the help of relativistic heavy ion collision experiments.

Many experimental results for particles at small transverse momentum can be understood in terms of relativistic fluid dynamics. As it turns out, heavy ion collisions at RHIC and LHC energies produce a rather strongly coupled liquid with a small ratio of shear viscosity to entropy density η/s. New data with improved statistics will provide more insights and better constraints in the coming years.

High momentum partons loose energy when traversing the dense QCD medium. A more detailed understanding of this effect is currently gained from reconstructed jets and more detailed data on nuclear modification factors.

Modifications of heavy quark bound state spectra in heavy ion collisions have been observed both for charm and bottom quarks. A more detailed quantitative understanding of this physics is work in progress.

Finally, other topics such as initial state physics, photons & di-leptons, the results from the low

energy run at RHIC and many more had to be skipped here for a lack of time but that does not make them less interesting in any way.

References

[1] E. V. Shuryak, "The QCD Vacuum, Hadrons and Superdense Matter", World Scientific, 2003.

[2] U. W. Heinz, "Concepts of heavy ion physics," hep-ph/0407360.

[3] J. I. Kapusta and C. Gale, "Finite-Temperature Field Theory", Cambridge University Press 2006.

[4] R. Vogt, "Ultrarelativistic Heavy-Ion Collisions", Elsevier 2007.

[5] W. Florkowski, "Phenomenology or Ultra-Relativistic Heavy-Ion Collisions", World Scientific, 2010.

[6] J. Casalderrey-Solana, H. Liu, D. Mateos, K. Rajagopal and U. A. Wiedemann, "Gauge/String Duality, Hot QCD and Heavy Ion Collisions," Cambridge University Press, Cambridge 2014.

[7] K. A. Olive *et al.* [Particle Data Group Collaboration], "Review of Particle Physics," Chin. Phys. C **38**, 090001 (2014). doi:10.1088/1674-1137/38/9/090001 and 2015 update.

[8] A. Andronic, P. Braun-Munzinger, K. Redlich and J. Stachel, "The statistical model in Pb-Pb collisions at the LHC," Nucl. Phys. A **904-905**, 535c (2013) doi:10.1016/j.nuclphysa.2013.02.070 [arXiv:1210.7724 [nucl-th]].

[9] J. Stachel, A. Andronic, P. Braun-Munzinger and K. Redlich, "Confronting LHC data with the statistical hadronization model," J. Phys. Conf. Ser. **509**, 012019 (2014) doi:10.1088/1742-6596/509/1/012019 [arXiv:1311.4662 [nucl-th]].

[10] P. Braun-Munzinger, J. Stachel and C. Wetterich, "Chemical freezeout and the QCD phase transition temperature," Phys. Lett. B **596**, 61 (2004) doi:10.1016/j.physletb.2004.05.081 [nucl-th/0311005].

[11] S. Floerchinger and C. Wetterich, "Chemical freeze-out in heavy ion collisions at large baryon densities," Nucl. Phys. A **890-891**, 11 (2012) doi:10.1016/j.nuclphysa.2012.07.009 [arXiv:1202.1671 [nucl-th]].

[12] Z. Fodor and S. D. Katz, "Critical point of QCD at finite T and mu, lattice results for physical quark masses," JHEP **0404**, 050 (2004) doi:10.1088/1126-6708/2004/04/050 [hep-lat/0402006].

[13] A. Andronic, P. Braun-Munzinger and J. Stachel, "The Horn, the hadron mass spectrum and the QCD phase diagram: The Statistical model of hadron production in central nucleus-nucleus collisions," Nucl. Phys. A **834**, 237C (2010) doi:10.1016/j.nuclphysa.2009.12.048 [arXiv:0911.4931 [nucl-th]].

[14] S. Borsanyi, G. Endrodi, Z. Fodor, A. Jakovac, S. D. Katz, S. Krieg, C. Ratti and K. K. Szabo, "The QCD equation of state with dynamical quarks," JHEP **1011**, 077 (2010) doi:10.1007/JHEP11(2010)077 [arXiv:1007.2580 [hep-lat]].

[15] P. B. Arnold, G. D. Moore and L. G. Yaffe, "Transport coefficients in high temperature gauge theories. 1. Leading log results," JHEP **0011**, 001 (2000) doi:10.1088/1126-6708/2000/11/001 [hep-ph/0010177].

[16] P. B. Arnold, C. Dogan and G. D. Moore, "The Bulk Viscosity of High-Temperature QCD," Phys. Rev. D **74**, 085021 (2006) doi:10.1103/PhysRevD.74.085021 [hep-ph/0608012].

[17] G. Policastro, D. T. Son and A. O. Starinets, "The Shear viscosity of strongly coupled N=4 supersymmetric Yang-Mills plasma," Phys. Rev. Lett. **87**, 081601 (2001) doi:10.1103/PhysRevLett.87.081601 [hep-th/0104066].

[18] P. Kovtun, D. T. Son and A. O. Starinets, "Viscosity in strongly interacting quantum field theories from black hole physics," Phys. Rev. Lett. **94**, 111601 (2005) doi:10.1103/PhysRevLett.94.111601 [hep-th/0405231].

[19] A. Buchel, "Transport properties of cascading gauge theories," Phys. Rev. D **72**, 106002 (2005) doi:10.1103/PhysRevD.72.106002 [hep-th/0509083].

[20] H. B. Meyer, "A Calculation of the shear viscosity in SU(3) gluodynamics," Phys. Rev. D **76**, 101701 (2007) doi:10.1103/PhysRevD.76.101701 [arXiv:0704.1801 [hep-lat]].

[21] H. B. Meyer, "Transport properties of the quark-gluon plasma from lattice QCD," Nucl. Phys. A **830**, 641C (2009) doi:10.1016/j.nuclphysa.2009.09.053 [arXiv:0907.4095 [hep-lat]].

[22] N. Christiansen, M. Haas, J. M. Pawlowski and N. Strodthoff, "Transport Coefficients in Yang–Mills Theory and QCD," Phys. Rev. Lett. **115**, no. 11, 112002 (2015) doi:10.1103/PhysRevLett.115.112002 [arXiv:1411.7986 [hep-ph]].

[23] M. Haas, L. Fister and J. M. Pawlowski, "Gluon spectral functions and transport coefficients in Yang–Mills theory," Phys. Rev. D **90**, 091501 (2014) doi:10.1103/PhysRevD.90.091501 [arXiv:1308.4960 [hep-ph]].

[24] S. Floerchinger and M. Martinez, "Fluid dynamic propagation of initial baryon number perturbations on a Bjorken flow background," Phys. Rev. C **92**, no. 6, 064906 (2015) doi:10.1103/PhysRevC.92.064906 [arXiv:1507.05569 [nucl-th]].

[25] S. Floerchinger and U. A. Wiedemann, "Mode-by-mode fluid dynamics for relativistic heavy ion collisions," Phys. Lett. B **728**, 407 (2014) doi:10.1016/j.physletb.2013.12.025 [arXiv:1307.3453 [hep-ph]].

[26] F. Cooper and G. Frye, "Comment on the Single Particle Distribution in the Hydrodynamic and Statistical Thermodynamic Models of Multiparticle Production," Phys. Rev. D **10**, 186 (1974). doi:10.1103/PhysRevD.10.186

[27] K. Aamodt *et al.* [ALICE Collaboration], "Suppression of Charged Particle Production at Large Transverse Momentum in Central Pb-Pb Collisions at $\sqrt{s_{NN}} = 2.76$ TeV," Phys. Lett. B **696**, 30 (2011) doi:10.1016/j.physletb.2010.12.020 [arXiv:1012.1004 [nucl-ex]].

[28] K. Aamodt *et al.* [ALICE Collaboration], "Elliptic flow of charged particles in Pb-Pb collisions at 2.76 TeV," Phys. Rev. Lett. **105**, 252302 (2010) doi:10.1103/PhysRevLett.105.252302 [arXiv:1011.3914 [nucl-ex]].

[29] G. Aad *et al.* [ATLAS Collaboration], "Measurement of the azimuthal anisotropy for charged particle production in $\sqrt{s_{NN}} = 2.76$ TeV lead-lead collisions with the ATLAS detector," Phys. Rev. C **86**, 014907 (2012) doi:10.1103/PhysRevC.86.014907 [arXiv:1203.3087 [hep-ex]].

[30] K. Aamodt *et al.* [ALICE Collaboration], "Higher harmonic anisotropic flow measurements of charged particles in Pb-Pb collisions at $\sqrt{s_{NN}}$=2.76 TeV," Phys. Rev. Lett. **107**, 032301 (2011) doi:10.1103/PhysRevLett.107.032301 [arXiv:1105.3865 [nucl-ex]].

[31] S. Floerchinger and U. A. Wiedemann, "Fluctuations around Bjorken Flow and the onset of turbulent phenomena," JHEP **1111**, 100 (2011) doi:10.1007/JHEP11(2011)100 [arXiv:1108.5535 [nucl-th]].

[32] C. Gale, S. Jeon, B. Schenke, P. Tribedy and R. Venugopalan, "Event-by-event anisotropic flow in heavy-ion collisions from combined Yang-Mills and viscous fluid dynamics," Phys. Rev. Lett. **110**, no. 1, 012302 (2013) doi:10.1103/PhysRevLett.110.012302 [arXiv:1209.6330 [nucl-th]].

[33] U. Heinz and R. Snellings, "Collective flow and viscosity in relativistic heavy-ion collisions," Ann. Rev. Nucl. Part. Sci. **63**, 123 (2013) doi:10.1146/annurev-nucl-102212-170540 [arXiv:1301.2826 [nucl-th]].

[34] S. Floerchinger, U. A. Wiedemann, A. Beraudo, L. Del Zanna, G. Inghirami and V. Rolando, "How (non-)linear is the hydrodynamics of heavy ion collisions?," Phys. Lett. B **735**, 305 (2014) doi:10.1016/j.physletb.2014.06.049 [arXiv:1312.5482 [hep-ph]].

[35] C. E. Coleman-Smith, H. Petersen and R. L. Wolpert, "Classification of initial state granularity via 2d Fourier Expansion," J. Phys. G **40**, 095103 (2013) doi:10.1088/0954-3899/40/9/095103 [arXiv:1204.5774 [hep-ph]].

[36] S. Floerchinger and U. A. Wiedemann, "Statistics of initial density perturbations in heavy ion collisions and their fluid dynamic response," JHEP **1408**, 005 (2014) doi:10.1007/JHEP08(2014)005 [arXiv:1405.4393 [hep-ph]].

[37] S. Floerchinger and U. A. Wiedemann, "Kinetic freeze-out, particle spectra and harmonic flow coefficients from mode-by-mode hydrodynamics," Phys. Rev. C **89**, no. 3, 034914 (2014) doi:10.1103/PhysRevC.89.034914 [arXiv:1311.7613 [hep-ph]].

[38] S. Chatrchyan *et al.* [CMS Collaboration], "Jet momentum dependence of jet quenching in PbPb collisions at $\sqrt{s_{NN}} = 2.76$ TeV," Phys. Lett. B **712**, 176 (2012) doi:10.1016/j.physletb.2012.04.058 [arXiv:1202.5022 [nucl-ex]].

[39] R. Baier, Y. L. Dokshitzer, A. H. Mueller, S. Peigne and D. Schiff, "Radiative energy loss of high-energy quarks and gluons in a finite volume quark - gluon plasma," Nucl. Phys. B **483**, 291 (1997) doi:10.1016/S0550-3213(96)00553-6 [hep-ph/9607355].

[40] B. G. Zakharov, "Fully quantum treatment of the Landau-Pomeranchuk-Migdal effect in QED and QCD," JETP Lett. **63**, 952 (1996) doi:10.1134/1.567126 [hep-ph/9607440].

[41] K. C. Zapp, F. Krauss and U. A. Wiedemann, "A perturbative framework for jet quenching," JHEP **1303**, 080 (2013) doi:10.1007/JHEP03(2013)080 [arXiv:1212.1599 [hep-ph]].

[42] K. C. Zapp, "JEWEL 2.0.0: directions for use," Eur. Phys. J. C **74**, no. 2, 2762 (2014) doi:10.1140/epjc/s10052-014-2762-1 [arXiv:1311.0048 [hep-ph]].

[43] T. Dahms [CMS Collaboration], "Quarkonia and heavy-flavour production in CMS," Nucl. Phys. A **910-911**, 91 (2013) doi:10.1016/j.nuclphysa.2012.12.017 [arXiv:1209.3661 [nucl-ex]].

[44] T. Matsui and H. Satz, "J/ψ Suppression by Quark-Gluon Plasma Formation," Phys. Lett. B **178**, 416 (1986). doi:10.1016/0370-2693(86)91404-8

[45] H. Satz, "Colour deconfinement and quarkonium binding," J. Phys. G **32**, R25 (2006) doi:10.1088/0954-3899/32/3/R01 [hep-ph/0512217].

[46] S. Chatrchyan *et al.* [CMS Collaboration], "Observation of sequential Upsilon suppression in PbPb collisions," Phys. Rev. Lett. **109**, 222301 (2012) doi:10.1103/PhysRevLett.109.222301 [arXiv:1208.2826 [nucl-ex]].